Electro–Mechano–Fluidic Modeling of Microsystems Using Finite Elements

V. Rochus[1], S. Gutschmidt[2], A. Cardona[3], and C. Geuzaine[4]

[1]IMEC, Leuven B3001, Belgium
[2]Department of Mechanical Engineering, University of Canterbury, Christchurch, New Zealand
[3]UNL, CIMEC-INTEC (UNL/CONICET) Santa Fe 3000, Argentina
[4]Department of Electrical Engineering and Computer Science (ACE), University of Liège, Liège B-4000, Belgium

Strong couplings between the mechanical, electric, magnetic, fluidic and thermal fields exist in the behaviour laws describing micro-systems. Also, due to the large surface/volume ratio, surface forces such as the electrostatic force and fluid damping become predominant. This paper presents the modeling and simulation of electrically-actuated micro-systems taking the electro-mechano-fluidic coupling into account. A micro-resonator consisting in a cantilever beam suspended over a substrate is modeled, and finite-element simulations are validated with experimental measurements.

***Index Terms*—Electromagnetic forces, electromechanical sensors, finite element methods, nonlinear dynamical systems, scientific computing.**

I. Introduction

FROM gas and pressure sensors to micro-pumps and micro-mirrors, micro–electro–mechanical systems (MEMS) are used in a large variety of sensors and actuators for automotive, biomedical, environment and space applications [1]. Current simulation technology only addresses the modeling and simulation of MEMS partially, often without satisfactorily solving the strongly coupled, multiscale and multiphysical problems at hand.

The aim of this paper is to present the modeling and simulation of electrically-actuated micro-systems using the finite-element method, focusing in particular on the strong coupling between the electrostatic actuation and the mechanical response, as well as on the modeling of fluid damping. This multiphysic modeling strategy is applied to the simulation of a micro-resonator consisting of a cantilever beam suspended over a substrate. The obtained numerical results are validated against experimental measurements.

II. Multi-Physical Modeling of MEMS

We use the finite-element method (FEM) to model the electro–mechanical–fluidic interactions and to perform static and dynamic analyses taking into account large mesh displacements and fluid damping. The usual method to model the coupling between electric and mechanical fields is to use two different numerical codes and iterate between them, which is time consuming and less accurate (e.g., for pull-in voltage computation [2]) when the coupling becomes stronger. Here we propose to compute electrical and mechanical fields and their interactions together in the same formulation.

A. Electro–Mechanical Coupling

A consistent way of deriving a finite-element discretization for the coupled electro–mechanical problem consists in applying the variational principle on the total energy of the coupled problem, which includes the electric and mechanical energies. The expression of the energy density results from thermodynamic considerations [3] and if the unknown variables are the mechanical displacement $\mathbf{u}$ and the scalar electric potential ϕ, *Gibb's free energy density* G has to be used [4]–[6]:

$$G = \frac{1}{2}\mathbf{S}^T\mathbf{T} - \frac{1}{2}\mathbf{D}^T\mathbf{E}, \tag{1}$$

where $\mathbf{S}(\mathbf{u})$ is the strain tensor, $\mathbf{T}(\mathbf{S})$ the stress tensor, $\mathbf{E}(\phi)$ the electric field and $\mathbf{D}(\mathbf{E})$ the electric displacement. The internal forces may be obtained using the virtual work principle as presented in [4].

The internal energy of the coupled problem on a volume Ω is:

$$W_{\text{int}} = \frac{1}{2}\int_\Omega \mathbf{S}^T\mathbf{T}\,d\Omega - \frac{1}{2}\int_{\Omega(\mathbf{u})} \mathbf{D}^T\mathbf{E}\,d\Omega = W_m - W_e \tag{2}$$

where W_m is the mechanical energy and W_e the electric co-energy. The total energy for the coupled problem, considering both internal and external contributions is

$$W = W_{\text{int}} - W_{\text{ext}}, \tag{3}$$

and the mechanical and electrical equilibrium are obtained by equating to zero the variations of the total energy (3) with respect to the displacement and the electric potential, i.e.,

$$\frac{\partial W}{\partial \mathbf{u}} \cdot \delta\mathbf{u} = 0 \quad \text{and} \quad \frac{\partial W}{\partial \boldsymbol{\phi}}\delta\phi = 0. \tag{4}$$

When developing (4) using (2) and (3), $(\partial W_m)/(\partial \mathbf{u})$ and $(\partial W_e)/(\partial \phi)$ can be treated as in the standard variational calculus for uncoupled electrostatics and mechanics. Further, the mechanical energy is independent from the electric potential: $(\partial W_m)/(\partial \phi) = 0$ (see [4]). The variation of the electric energy due to the displacement $\mathbf{u}$ is the contribution of the electrostatic forces. After some developments [4], we obtain

$$\frac{\partial W_e}{\partial \phi}\delta\mathbf{u} = \frac{1}{2}\int_\Omega \mathbf{D}^T\mathbf{F}\mathrm{grad}\delta\mathbf{u}\,d\Omega \tag{5}$$

where $\mathbf{F}(\nabla\phi)$ is a matrix depending on the space derivatives of ϕ. This term represents the electrostatic forces on the structure. From (4) and (5), a fully coupled finite-element formulation can be built following classical discretization procedures.

Manuscript received July 05, 2011; accepted October 21, 2011. Date of current version January 25, 2012. Corresponding author: C. Geuzaine (e-mail: cgeuzaine@ulg.ac.be).

Color versions of one or more of the figures in this paper are available online at http://ieeexplore.ieee.org.

Digital Object Identifier 10.1109/TMAG.2011.2173663

0018-9464/$31.00 © 2012 IEEE

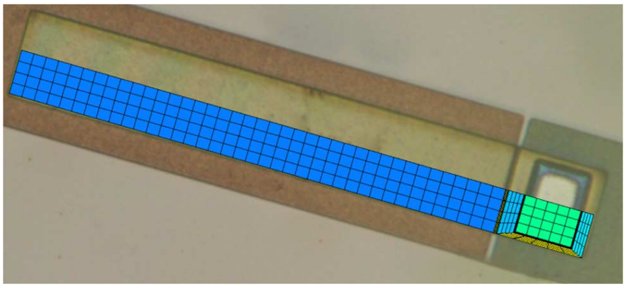

Fig. 1. Finite-element mesh superimposed with a microscope photograph of the micro-resonator (viewed from above).

The variation of the mechanical and electrostatic forces with respect to small potential and displacement perturbations is an important characteristic of the coupled system since it allows a better convergence of static nonlinear solvers and a better evaluation of the linear vibrations around equilibrium positions [2]. The tangent stiffness matrix around a position $(\mathbf{u}_0, \phi_0)$ may be obtained by linearization of the internal forces. The finite-element form is

$$\begin{pmatrix} \mathbf{K}_{uu}(\phi) & \mathbf{K}_{u\phi}(\phi) \\ \mathbf{K}_{\phi u}(\phi) & \mathbf{K}_{\phi\phi} \end{pmatrix} \begin{pmatrix} \Delta\mathbf{U} \\ \Delta\mathbf{\Phi} \end{pmatrix} = \begin{pmatrix} \Delta\mathbf{F_m} \\ \Delta\mathbf{Q} \end{pmatrix} \tag{6}$$

where $\mathbf{U}$ and $\mathbf{\Phi}$ are the discretized displacement and potential fields $\mathbf{u}$ and ϕ and $\mathbf{F_m}$ and $\mathbf{Q}$ are the discretized external sources. The total coupled matrix is symmetric. The matrix $\mathbf{K}_{\phi\phi}$ is the stiffness matrix of the purely electric problem. The remaining terms are derived from the total energy as presented in [4]. These terms depend on the electric field and the coupled problem is thus nonlinear.

B. Squeeze Film Damping

The structures considered here are cantilever micro-beams suspended over a substrate as shown in Fig. 1. To model the effects of the air squeezed in the gap between the beam and the substrate, the nonlinear Reynolds equation is considered:

$$\frac{\partial}{\partial x_i}\left(\frac{ph^3}{12\mu}\frac{\partial p}{\partial x_i}\right) = \frac{\partial(ph)}{\partial t} \tag{7}$$

where p is the total pressure, h is the gap (the distance between the two plates), and μ the air viscosity. This relation is valid only if the flow is laminar and fully developed, if the pressure is constant along the z-direction and if the fluid does not slip at the wall [7]. Another important assumption of this model is the continuum assumption of fluid mechanics: if the dimensionless Knudsen number $K_n = \lambda/h > 1$, where λ is the mean-free path of the molecules in the gas, (7) is not valid anymore and should be replaced by a statistical model. When $K_n \approx 1$, which often happens in MEMS, (7) can still be used provided that a modified viscosity $\mu = (\mu_0)/(1+9.638K_n^{1.159})$ is considered, where μ_0 is the viscosity at atmospheric pressure [8].

In the case of perforated micro-structures as the structure presented in Fig. 6, a new term can be added in (7) to take the release of the fluid through the holes into account. The equation is then called the perforation profile Reynolds equation (PPR) [9]. This hole effect is modeled by the perforation acoustic impedance Z which depends on the hole size, the distance between the holes, the gap and the thickness of the structure. In the case of large holes compared to the thickness and the gap, the complete lumped model proposed in [10] has to be used to determine the impedance.

To obtain the weak form, the PPR equation is premultiplied by a test function δp

$$\int_\Omega \delta p \left(\frac{\partial}{\partial x_i}\left(\frac{ph^3}{12\mu}\frac{\partial p}{\partial x_i}\right) - \frac{\partial(ph)}{\partial t} + \frac{p_0}{Z}p\right) dV = 0 \tag{8}$$

where p_0 is the external pressure. The coupling with the mechanics comes from the dependency of the gap on the displacement $h = h_0 + (\mathbf{u}.\mathbf{n})$, where $\mathbf{n}$ is the surface normal, and the action of the fluid pressure on the structure modeled by the mechanical damping force $\mathbf{f}_{fl} = \int_S p\,\mathbf{n}\,dS$ where $\mathbf{n}$ is the surface normal. After discretization, the finite-element fluidic formulation becomes

$$\mathbf{C}_{pp}(h)\dot{\mathbf{P}} + \mathbf{K}_{pp}(h,p)\mathbf{P} + \mathbf{C}_{pu}(p)\dot{\mathbf{U}} = \mathbf{0} \tag{9}$$

where $\mathbf{P}$ is the discretized pressure and $\mathbf{C}_{pp}$, $\mathbf{C}_{pu}$ and $\mathbf{K}_{pp}$ are coupling matrices depending on the gap and the pressure [11], [12], and the hole release term is included in the matrix $\mathbf{K}_{pp}$.

III. Multi-Physic Solvers

A. Static Solver

To compute the static equilibrium, the system of equations is reduced to the coupling between mechanics and electrostatics. The residue to cancel is

$$\mathbf{r}(\mathbf{u},\phi) = \begin{cases} \mathbf{K}_{uu}\mathbf{U} - \mathbf{F}_e(\mathbf{u},\boldsymbol{\phi}) - \mathbf{F}_m \\ \mathbf{K}_{\phi\phi}\mathbf{\Phi} - \mathbf{Q} \end{cases}, \tag{10}$$

where $\mathbf{F}_e$ are the discretized electrostatic forces and $\mathbf{F}_m$ are the external mechanical forces. This equation being nonlinear, an iterative solution method is needed. Starting at the nth step, which is a known equilibrium position $\mathbf{z}_n^* = (u_n^*, \phi_n^*)$, to get to the $(n+1)$th equilibrium step, a prediction phase $\mathbf{z}_{n+1}^0$ is generated. Then, following the continuation algorithm, the ith iteration solution is obtained [13] by

$$\begin{cases} \dfrac{\partial\mathbf{r}\left(\mathbf{z}_{n+1}^{i-1}\right)}{\partial\mathbf{z}}\Delta\mathbf{z} = -r(\mathbf{z}_{n+1}^{i-1}) \\ \mathbf{c}\left(\mathbf{z}_{n+1}^i\right) = 0 \end{cases} \tag{11}$$

where $\Delta\mathbf{z} = \mathbf{z}_{n+1}^i - \mathbf{z}_{n+1}^{i-1}$ and $\mathbf{c}$ is an auxiliary constraint equation which depends on the chosen continuation algorithm. In the case of the Crisfield algorithm [13], $\mathbf{c}(\mathbf{z}_{n+1}^i) = (\mathbf{z}_{n+1}^i - \mathbf{z}_n^*)^2 - l^2 = 0$. The derivative of the residue by the variables $(\partial\mathbf{r}(\mathbf{z}_{n+1}^{i-1}))/(\partial\mathbf{z})$ corresponds to the tangent stiffness matrix obtained in (6).

B. Harmonic Solver

Around the static equilibrium (u_n^*, ϕ_n^*), a harmonic solver is applied to determine the dynamic behavior of the system taking the fluid damping into account. The electro–mechano–fluidic dynamic equations are as follows:

$$\begin{cases} \mathbf{M}\ddot{\mathbf{U}} + \mathbf{K}_{uu}\mathbf{U} = \mathbf{F}_e(\mathbf{u},\phi) + \mathbf{F}_{fl}(p) + \mathbf{F}_m \\ \mathbf{K}_{\phi\phi}\mathbf{\Phi} = \mathbf{Q} \\ \mathbf{C}_{pp}\dot{\mathbf{P}} + \mathbf{K}_{pp}\mathbf{P} + \mathbf{C}_{pu}\dot{\mathbf{U}} = 0 \end{cases} \tag{12}$$

where $\mathbf{F}_{fl}$ is the discretized fluidic damping force. The linearization of these equations around an equilibrium position

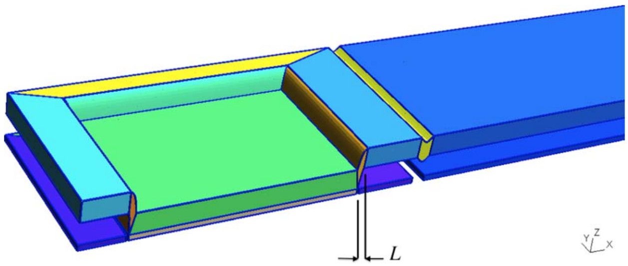

Fig. 2. Detail of the micro-beam anchor.

(u_n^*, ϕ_n^*) provides the different terms needed to use a standard harmonic solver:

$$\begin{pmatrix} \mathbf{M} & 0 & 0 \\ 0 & 0 & 0 \\ 0 & 0 & 0 \end{pmatrix} \begin{pmatrix} \Delta\ddot{\mathbf{U}} \\ \Delta\ddot{\mathbf{\Phi}} \\ \Delta\ddot{\mathbf{P}} \end{pmatrix} + \begin{pmatrix} 0 & 0 & 0 \\ 0 & 0 & 0 \\ \mathbf{C}_{pu} & 0 & \mathbf{C}_{pp} \end{pmatrix} \begin{pmatrix} \Delta\dot{\mathbf{U}} \\ \Delta\dot{\mathbf{\Phi}} \\ \Delta\dot{\mathbf{P}} \end{pmatrix} + \begin{pmatrix} \mathbf{K}_{uu} & \mathbf{K}_{u\phi} & \mathbf{K}_{up} \\ \mathbf{K}_{\phi u} & \mathbf{K}_{\phi\phi} & 0 \\ 0 & 0 & \mathbf{K}_{pp} \end{pmatrix} \begin{pmatrix} \Delta\mathbf{U} \\ \Delta\mathbf{\Phi} \\ \Delta\mathbf{P} \end{pmatrix} = \begin{pmatrix} \Delta\mathbf{F_m} \\ \Delta\mathbf{Q} \\ \Delta\mathbf{P_f} \end{pmatrix}. \quad (13)$$

IV. Simulations and Experimental Measurements

The examples studied here are micro-resonators consisting of a cantilever beam suspended over a lower electrode deposited on the substrate see Fig. 1. The technology used for fabrication is the PolyMUMPS process proposed by MEMSCAP. The beams are made of polysilicon. The Young modulus is estimated at 158 ± 10 GPa, the Poisson coefficient is 0.22 ± 0.01 and the mass density is 2330 kg/m^3. The resonator is placed in air with a viscosity of 18 10^{-6} Pa.s at atmospheric pressure (10^5 Pa).

A. 175 μm Cantilever Beam

The considered beam measures 175 μm $\times$ 2 μm $\times$ 30 μm. The air gap between the beam and the lower electrode is about 2 μm and the lower electrode starts at 7 μm from the anchor. Its initial deflection being nearly zero, the prestress due to fabrication is neglected. Fig. 1 shows a top view of the resonator together with the finite-element mesh modeling the structure. The mechanical structure is modeled by nonconforming nonlinear elements taking the large displacement hypothesis into account [14]. Fig. 2 shows in more details the geometrical model of the beam anchor. Since the anchor shape cannot be measured accurately experimentally, the geometrical design is defined as close as possible to the reality based on scanning electron microscope images.

Fig. 3 compares the static response with experimental data. The strongly coupled electro–mechanical problem is solved using the Crisfield continuation algorithm to obtain the equilibrium position for each voltage. A study is performed to determine the anchor shape by defining two design parameters: L, the tilt of the anchor and r, the deposition thickness on a vertical edge as presented in Fig. 3. The anchor shape has clearly an important influence on the behavior of the structure. One set of optimal values for these parameters is $r = 0.5$ μm and $L = 1.5$ μm.

Keeping this optimal design, the dynamic response is then compared to experimental measurements as presented in Fig. 4. The resonance frequencies are measured experimentally using a vibrometer analyzer POLYTEC MSA400 [15] by applying a ac and a dc voltage to the resonator. First the structure is excited by a dc voltage of 5 V, which bends the beam (statically). An ac voltage is then superimposed to the dc voltage according to the input signal plotted in Fig. 4. This white noise signal has a frequency spectrum ranging from 0 to 500 kHz and a discrete Fourier transform mean intensity of 0.027 V, with minimal and maximal values of 0.024 and 0.03 V. To simulate this excitation numerically, a static analysis is first performed for $V_{\mathrm{dc}} = 5$ V as presented previously. Then, the harmonic response is computed around this position for three ac voltages: 0.024 V (pink line), 0.027 V (black line, the mean value), and 0.03 V (blue line). As observed in Fig. 4, the amplitude of the ac voltage has a big influence on the dynamic results. Despite the rather simple fluid damping model, the experimental resonance frequencies match the numerical simulations quite well.

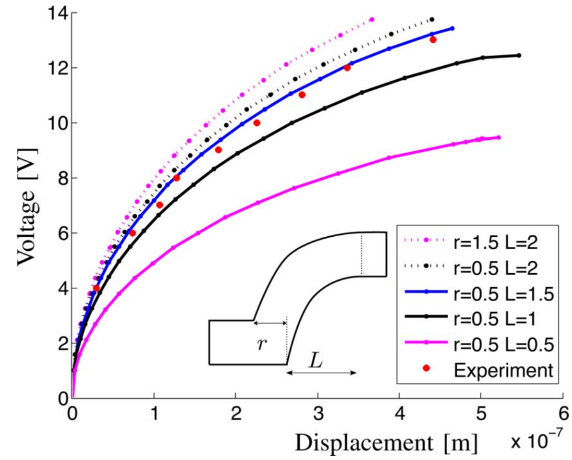

Fig. 3. Applied voltage [V] versus displacement of the tip of the beam [m] for different values of the length L of the anchor connection (see Fig. 2).

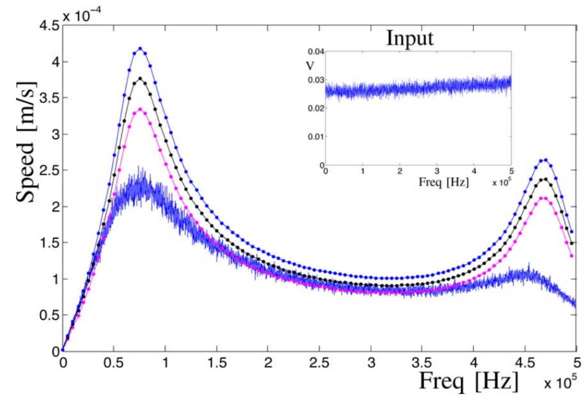

Fig. 4. Dynamic response of the micro-resonator: speed of the tip of the beam [m/s] versus frequency [Hz] when a dc voltage of 5 V and an white noise voltage of 0.024 V (pink line), 0.027 V (black line), and 0.03 V (blue line) are applied. The jagged curve denotes the experimental values.

B. 200 μm Cantilever Beam

To validate the parameters chosen to model the anchor of the 175 μm beam, the same simulations are performed for a 200 μm $\times$ 2 μm $\times$ 30 μm cantilever beam for a continuous voltage V_{dc} of 5 V and a mean ac amplitude of $V_{\mathrm{ac}} = 0.023$ V. The input graph depicted in Fig. 5 does not show the constant characteristic which would have been ideal. Thus, results for higher frequency have to be handled with care. The dynamic behavior of the 200 μm micro-resonator is then studied for

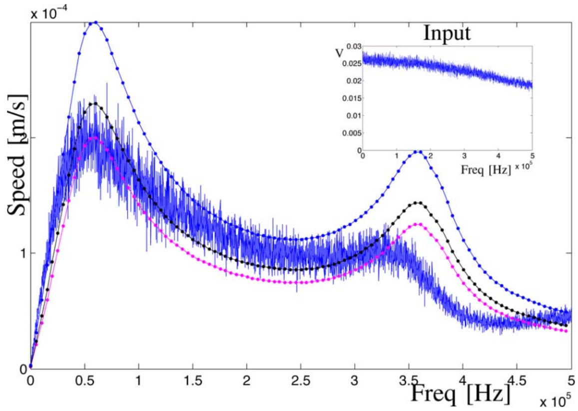

Fig. 5. Dynamic response of a 200 μm micro-resonator: speed of the tip of the beam [m/s] versus frequency [Hz] when a dc voltage of 5 V and an white noise voltage of 0.02 V (pink line), 0.023 V (black line, mean value), and 0.027 V (blue line) are applied. The jagged curve denotes the experimental values.

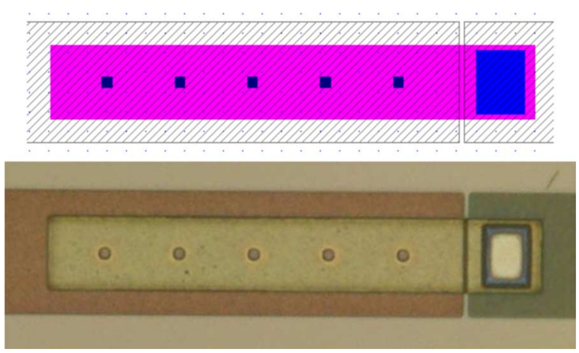

Fig. 6. Layout and photography of the holed 175 μm beam.

$V_{\rm ac} = 0.02$ V, 0.023 V, and 0.027 V. Again, the experimental response fits quite well with the curve for $V_{\rm ac} = 0.027$ V, especially in the lower part of the frequency range as is expected for the applied input signal.

C. 175 μm Cantilever Beam With Holes

Finally the dynamic behavior of a holed 175 μm $\times$ 2 μm $\times$ 30 μm micro-resonator is studied around its static equilibrium of 5 V and with a mean ac amplitude of 0.024 V. This beam comprises 5 holes of 4 μm length as shown in Fig. 6. The size of the holes being larger than the gap and the thickness of the beam, the complete lumped model proposed by Veijola [10] has to be used to estimate the acoustic impedance Z and the obtained value is $Z = 1.2$e6 Pa.s/m. The dynamic simulations are then performed for $V_{\rm ac}$ of 0.02 V (pink line), 0.024 V (black line), and 0.03 V (blue line) and plotted in Fig. 7. The dashed black line corresponds to numerical results for $V_{\rm ac} = 0.024$ V without considering the damping in the holes. Again the first resonance frequency is well fitted.

V. Conclusion

This paper presents the modeling of micro-resonators taking the electro-mechano-fluid coupling into account. First a static analysis is performed using the Crisfield algorithm to identify the shape of the anchor, fitting the numerical results to experimental measurements. We found that $L = 1.5$ μm and $r = 0.5$ μm represents a good fit with experiments. Then harmonic numerical results are compared to experiments to verify the damping model. We observe a strong influence of the

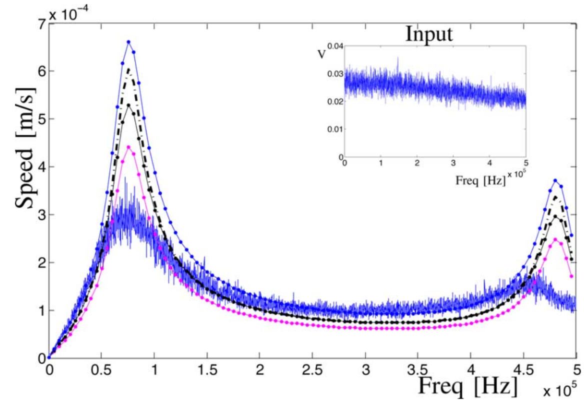

Fig. 7. Dynamic response of the holed micro-resonator : speed of the tip of the beam [m/s] versus frequency [Hz] when a dc voltage of 5 V and an white noise voltage of 0.02 V (pink line), 0.024 V (black line, mean value), and 0.03 V (blue line) are applied. The jagged curve denotes the experimental values.

input voltage on the results. Then the same anchor shape is used for other micro-resonators: a 200 μm resonator and a 175 μm micro-beam with holes. Again the experimental measurements fit the numerical results well, validating the parameters used to model the anchor.

Acknowledgment

This work has been performed in the framework of the projet Secyt-FNRS "Numerical Simulation in Microeletromechanics (MEMS)". The first author acknowledges the financial support of the Belgian National Fund for Scientific Research.

References

[1] S. Senturia, *Microsystem Design*. Norwell, MA: Kluwer, 2001.
[2] V. Rochus, "Advantages of an energetic approach to derive the electro-mechanical coupling," *Sensor Lett.*, vol. 6, no. 1, pp. 88–96, 2008.
[3] T. Ikeda, *Fundamentals of Piezoelectricity*. London, U.K.: Oxford Univ. Press, 1996.
[4] V. Rochus, D. J. Rixen, and J.-C. Golinval, "Monolithic modeling of electro-mechanical coupling in micro-structures," *Int. J. Numer. Methods Eng.*, vol. 65/4, pp. 461–493, 2006.
[5] V. Rochus, E. Lemaire, and C. Geuzaine, "Dual approach for an accurate estimation of pull-in voltage," in *Proc. IVth Eur. Conf. Comput. Mechan. (ECCM)*, 2010.
[6] V. Rochus and C. Geuzaine, "A primal/dual approach for the accurate evaluation of the electromechanical coupling in MEMS," *Finite Elements Anal. Des.*, vol. 49, no. 1, Feb. 2012.
[7] M. Bao and H. Yang, "Squeeze film air damping in MEMS," *Sens. Actuators: A, Phys.*, vol. 136/1, pp. 3–27, 2007.
[8] T. Veijola, H. Kuisma, J. Lahdenperä, and T. Ryhänen, "Equivalent-circuit model of the squeezed gas film in a silicon accelerometer," *Sens. Actuators A, Phys.*, vol. 48/3, pp. 239–248, 1995.
[9] Y. J. Yang and C. J. Yu, "Macromodel extraction of gas damping effects for perforated surfaces with arbitrarily-shaped geometries," in *Proc. 5th Int. Conf. Model. Simulat. Microsyst.*, 2002, pp. 178–181.
[10] T. Veijola and P. Raback, "Methods for solving gas damping problems in perforated microstructures using a 2-D finite-element solver," *Sensors*, vol. 7, pp. 1069–1090, 2007.
[11] J. Barroso, O. Bruls, C. Berli, and A. Cardona, "Modelling of the squeeze film air damping in MEMS," in *Proc. ENIEF Conf.*, 2009.
[12] S. D. A. Hannot and D. J. Rixen, "Building and reducing a three-field finite-element model of a damped electromechanical actuator," *J. Microelectromech. Syst.*, vol. 20, no. 3, pp. 665–675, 2011.
[13] S. A. Ragon, Z. Gürdal, and L. T. Watson, "A comparison of three algorithms for tracing nonlinear equilibrium paths of structural systems," *Int. J. Solids Struct.*, vol. 39/3, pp. 689–698, 2002.
[14] V. Rochus, D. J. Rixen, and J. C. Golinval, "Non-conforming element for accurate modelling of MEMS," *Finite Elements Anal. Des.*, vol. 43, pp. 749–756, 2007.
[15] S. Gutschmidt, V. Rochus, and J. C. Golinval, "Static and dynamic experimental investigations of a micro-electromechanical cantilever in air and vacuum," in *Proc. EuroSimE IEEE Conf.*, 2009.